

# Partial persistence of memory in bubble breakup: incomplete universality acquired by broken symmetry

Ikumi Yoshino and Ko Okumura\*

Physics Department and Soft Matter Center, Ochanomizu University, 2-1-1 Ohtsuka, Bunkyo-ku, Tokyo 112-8610, Japan

(Dated: June 17, 2025)

When a water drop falls from a faucet, the drop is created with the formation of an axisymmetric constriction region, which thins down to breakup. Such formation of a fluid drop has been extensively studied as a representative case of the singular dynamics widely observed in nature. The singular dynamics is often self-similar: shape at different times collapsing onto a master curve after rescaling. The self-similar dynamics has been categorized as either universal or non-universal: the master curve is independent from or dependent on the length scales that set the initial boundary conditions, as if memory is erased or retained. In the previously known cases, where the axisymmetry is maintained, only a single length scale is available for the boundary conditions, a tube radius, and, thus, there is no possibility of partial memory. Here, we focus on the post-breakup and confine the system to break the axisymmetry, introducing three length scales, which leads to a third category of incomplete universality, where memory is partially retained: the master curve for the post-breakup is dependent on the smallest scale but independent from the other two scales. Affecting of only the smallest length scale on the master curve underscores the importance of scale separation for the emergence of universality: near the singularity physics at small scales becomes important. The present study suggests a promising direction for the study on the singular dynamics by exploring the symmetry and has implications for bubble/drop generation in confined geometries, encountered in various fields from microfluidics to geology.

Singular dynamics observed widely in nature from the gravitational collapse of a star [1] to the formation of a drop in dripping faucets [2] have attracted scientist in many fields such as cosmology [3], hydrodynamics, physics and mathematics [4, 5]. One important feature of the singular dynamics governed by partial differential equations is *self-similarity or scale-invariance*, i.e., the shapes at different times can be superimposed onto a master curve by rescaling, as observed in various phenomena including fluid-jet formation [6, 7] and drop coalescence [8–10]. The self-similar dynamics is said to be *universal* and *losing memory*, when the master curve representing the self-similarity is independent of the scales that set the initial boundary conditions with remaining dependence on only a few material parameters. This scenario is expected from separation of scales: the physics at small scales in length and time becomes so important that the dynamics does not exhibit any dependence on larger scales such as those setting the boundary conditions. One example of the *self-similar and universal dynamics* is the breakup of a drop surrounded by less viscous fluid, where capillarity, inertia, and viscosity all come into play [11]. However, the breakup of bubble surrounded by more viscous fluid was shown to be *self-similar but non-universal*, where the dynamics governed by the Stokes equation describing the viscous-capillary balance, which does not define internal length scales [12]: the master curve representing the self-similarity does depend on the boundary condition, *retaining memory*. In addition, the crossover from universal to non-universal self-similar dynamics is reported for the pinch-off of a bubble in a tube [13], where both regimes are governed by capillarity and viscosity and the universal regime is

described by a wetting rim dynamics.

Here, we focus on the post-breakup dynamics and report a novel scenario in the singular dynamics as a result of a viscosity-gravity balance: *the incomplete universality where memory is partially retained*. The key is a confinement, which involves a few length scales and breaks the axisymmetry of the previous cases, which allow only one length that sets the boundary conditions, i.e., a tube radius. In the present case, however, we have three independent length scales for the boundary conditions. As a result, we found the master curve, by which the self-similar dynamics is represented, does depend on the smallest length but not on the other scales, which is natural from the viewpoint of separation of scales. We show this new class of the singular dynamics by experiments with a high quality. The novel scenario of the incomplete universality on the memory in singular dynamics revealed in the present study opens a new avenue for understanding singular dynamics widely observed in nature and underscores the importance of exploration of the symmetry in singular dynamics.

## I. RESULTS

### A. Experimental

In Fig. 1 (a), we show our experimental setup with explanation. The cell width and height are much larger than the length scales  $R$ ,  $D_0$ , and  $D$  (typically 9 and 12 cm, respectively). We use polydimethylsiloxane (PDMS) for viscous liquid of kinematic viscosity  $\nu = \eta/\rho$ . The density  $\rho$  and the surface tension  $\gamma$  are slightly depending

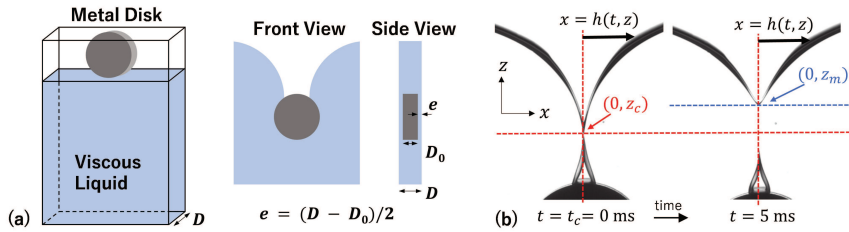


FIG. 1. (a) Experimental setup. A metal disk of thickness  $D_0$  ( $= 2.0 - 3.5$  mm) and radius  $R$  (10 to 15 mm) falls in the cell of thickness  $D$  (3 to 4.5 mm) filled with a viscous liquid of kinematic viscosity  $\nu$  (1 to 50 St). The disk entrains air into the liquid, which finally detaches from the disk. The difference between  $D$  and  $D_0$  defines the liquid film thickness  $e$ . (b) Snapshots at breakup and after breakup illustrating the setting of axes for  $(e, D_0, R, \nu) = (0.5, 3, 10, 1)$  in mm or St.  $z = z_c$  is set to the origin of the  $z$  coordinate.

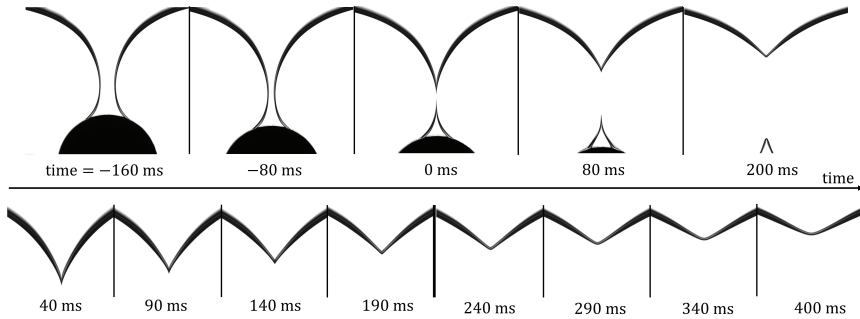


FIG. 2. Snapshots of entrainment of air by a disk into liquid, leading to breakup of a sheet of air for  $(R, D_0, e, \nu) = (10, 3, 0.5, 10)$  in mm or St. In the top panel, overall time development is shown. In the bottom magnified snapshots, we recognize that the sharp tip at short times become rounded with time, with the thick vertical line in the middle indicates the border. The time label 0 ms corresponds to  $t = t_c$  defined in the text.

on viscosity  $\eta$  ( $\rho \simeq 0.97$  g/cm $^3$  and  $\gamma \simeq 20$  mN/m). The density  $\rho_s$  of the metal disk is either is 7.7 g/cm $^3$  (stainless: SUS430) or 8.7 g/cm $^3$  (brass) with the density difference  $\Delta\rho = \rho_s - \rho$ . The cell is fabricated with acrylic plates of thickness 5 mm, using acrylic spacers whose thickness defines the cell thickness  $D$ . For further details, see Appendix A.

## B. Temporal change of the dynamics

In Fig. 2, we show typical snapshots before and after breakup in the present parameter range. A thin air film is formed slightly before breakup, as confirmed by the side-view snapshots obtained for a similar parameter set in our previous study on the pre-breakup dynamics [14]. In the post breakup of the present focus, the tip is sharp when seen from the front as in the snapshots at short times (just after the breakup), but becomes rounded with time, while our focus below is mainly on the regime after the breakup but before the tip becomes clearly rounded.

## C. Shape of the air-liquid interface $h(z, t)$

We explain the definition of the shape and the setting of space-time coordinate (see Fig. 1 (b)). The shape of air-liquid interfaces formed by air entrained by the disk are seen as the dark line with a finite thickness. In the present study, the inner edge of the right (or left) line is described by:  $x = h(z, t)$  (or  $-h(z, t)$ ). For further details, see Appendix B.

The space-time coordinate is determined as follows (see Fig. 1 (b)). Before breakup the function  $h(z, t)$  possesses a minimum with respect to  $z$ , which we call "the constriction point," at which  $(x, z) = (h_m(t), z_m(t))$ , i.e.,  $h_m(t) = h(z_m(t), t)$ . At  $t = t_c$ , topology changes: The fluid breaks into two chunks at the constriction point  $(h_m(t_c), z_m(t_c)) = (0, z_c)$ , where  $z = z_c$  will be set to the origin of the  $z$  coordinate. After  $t = t_c$ , the constriction point thus disappears and the dynamics of the interface of our focus is characterized by the tip point  $(0, z_m - z_c) = (0, z_m)$ . Experimentally, our time label 0 ms could deviate from the true  $t = t_c$  at most 1 ms, which is set by frames per second in capturing images. See further details for Appendix B.

The way of the selection the edge and the determination of time label 0 ms, detailed in Appendix B is technically important for data collapse presented below. Slight

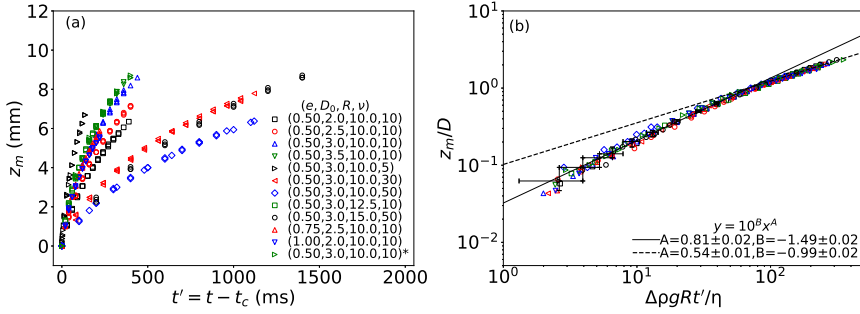


FIG. 3. (a)  $z_m$  vs.  $t' = t - t_c$ , where  $t_c$  is the critical time defined in the text for various parameters  $(e, D_0, R, \nu)$  in mm or St. The data marked with a star (\*) in the legend are those obtained for a different  $\Delta\rho$  by using a brass disk instead of a disk of stainless steel. (b) Distinct data collapse by Eq. (1). All the data in (a) are plotted on rescaled axes, based on Eq. (1), demonstrating a clear data collapse with a quasi scaling-crossover between the regimes reasonably well characterized by the exponent  $\Delta' \simeq 0.8$  and  $1/2$ .

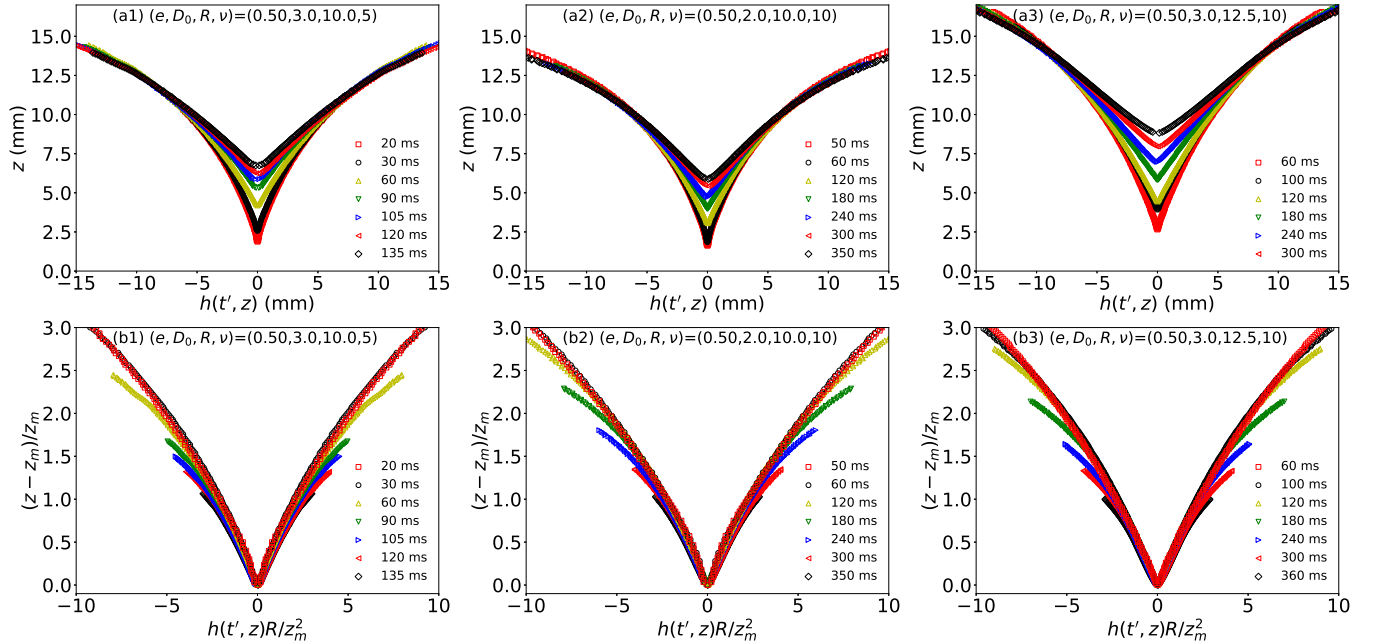


FIG. 4. (a1) to (a3) Temporal change of the interface  $h(z, t)$  at  $e = 0.5$  mm for the parameter sets  $(D_0, R, \nu) = (3, 10.0, 0.5)$ ,  $(1.0, 10.0, 10)$  and  $(2.0, 12.5, 10)$  in mm or St. The error bars in capturing the interface are less than the size of markers. (b1) to (b3) The space-time dependent collapse of the shape by Eq. (2). The collapse near the tip persists for long time, while that away from the tip is observed only for short time.

changes could deteriorate the quality of the collapse.

#### D. Dynamics of characteristic length scale

In Fig. 3 (a), we present the relation between  $z_m$  and  $t$  for various conditions, in which we can confirm an excellent reproducibility of the present measurement. For example, if we closely examine the data shown by blue diamond, we see several overlapping data points, which are generally obtained on different days.

In Fig. 3 (b), in which we show error bars for a set of data, we can confirm all the data in (a), which include the data for different  $e$ ,  $D_0$ ,  $R$ ,  $\eta$ , and  $\Delta\rho$ , can be well

described by the following relation between dimensionless quantities:

$$z_m(t)/D = f(\Delta\rho g R t'/\eta) \equiv f(t'/\tau) \quad (1)$$

with  $\tau = \eta/\Delta\rho g R$ , where a time label  $t'$  (which is positive at times after  $t = t_c$ ) is defined as  $t' = t - t_c$ . The data for the brass disk in Fig. 3 (b) are separately shown in Fig. 6 (b3) below, together with the corresponding data obtained by the stainless disk and the fitting lines, to show clear dependence on  $\Delta\rho$ . We can further confirm in Fig. 3 (b) that the slope  $\Delta'$  of the  $z_m$ - $t'$  relation on log-log scales seem to exhibit a crossover from Regime I to Regime II:  $\tilde{z}_m = \tilde{t}^{\Delta'}$  with  $\tilde{z}_m = z_m/D$  and  $\tilde{t} \simeq t'/\tau$ , where  $\Delta' \simeq 0.8$  in Regime I and  $\Delta' \simeq 1/2$  in Regime

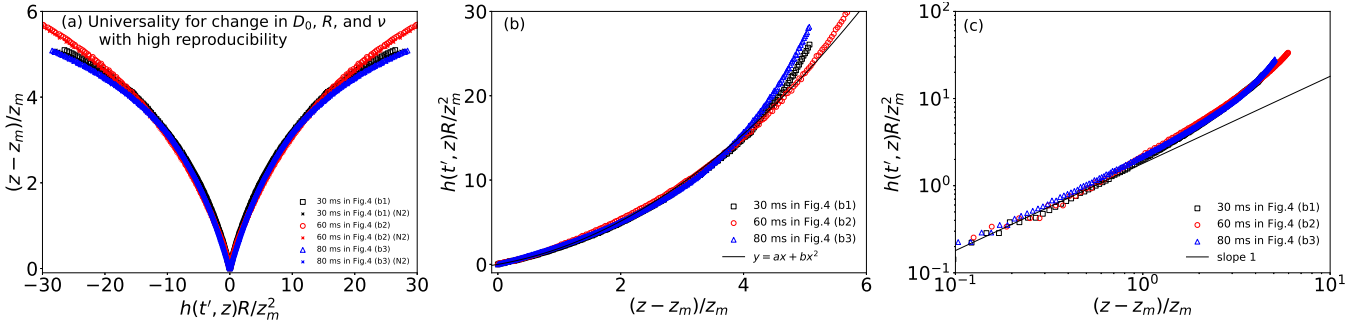


FIG. 5. (a) The master curves universal (and highly reproducible) for change in  $D_0$ ,  $R$ , and  $\nu = \eta/\rho$  at  $e = 0.5$  mm (but non-universal for change in  $e$  and  $\Delta\rho$ , as shown below in Fig. 6 (a3)). Shapes at earlier times in Fig. 4 are compared. The data marked as (N2) are basically obtained on a different day. (b) Right branches in (a) are shown with fitting based on Eq. (3) with the axes interchanged. (c) Plot in (b) on log-log scales.

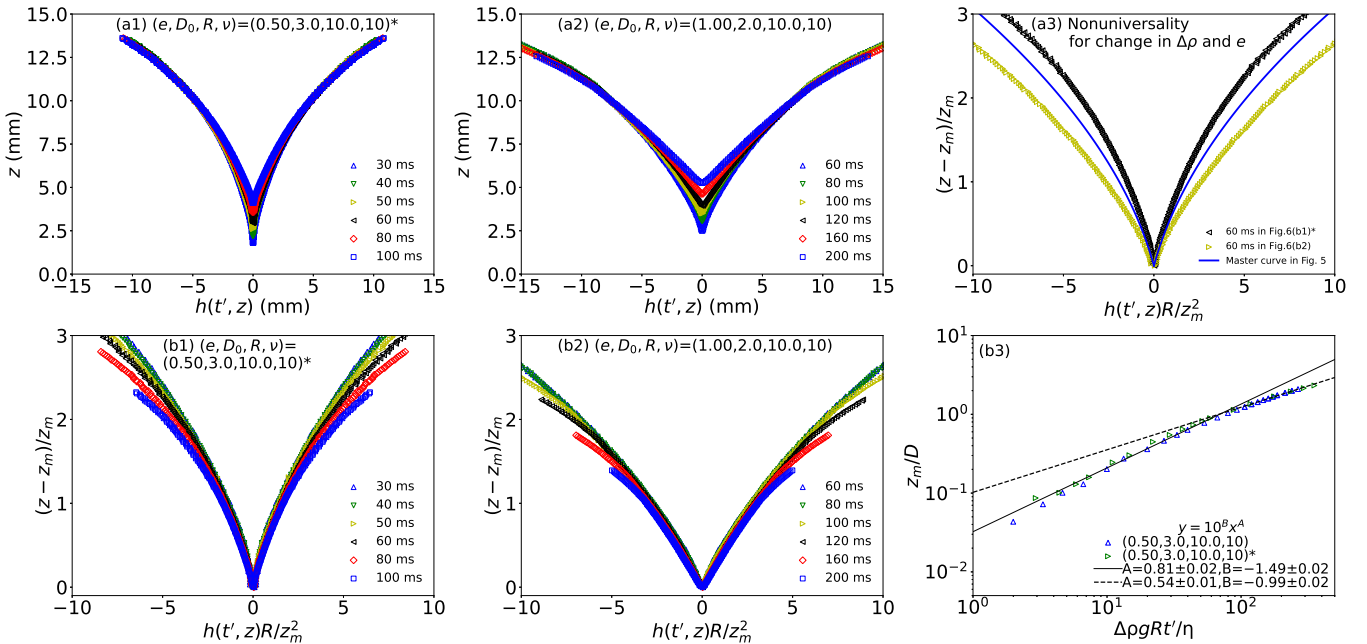


FIG. 6. (a1) and (a2) Temporal change of the interface  $h(z, t)$  at  $\Delta\rho$  and  $e$  different from those in Fig. 4 or Fig. 5:  $(e, D_0, R, \nu) = (0.5, 3, 10, 10)$  in mm or St using a brass disk and  $(1.0, 2.0, 10, 10)$  using a stainless disk. The star (\*) in (a1) [as well as in (b1), (a3) and (b3) below] indicates the data obtained for different  $\Delta\rho$  as in Fig. 3. (b1) to (b2) The space-time dependent collapse of the shape by Eq. (2). (a3) The master curves non-universal for change in  $e$  and  $\Delta\rho$ . Shapes in (b1) and (b2) at an earlier time are compared with the master curve (precisely, the fitting line) in Fig. 5 (b). (b3)  $z_m$  vs.  $t' = t - t_c$ . We extract from Fig. 3 (b) the data obtained for two different  $\Delta\rho$ 's (using the stainless and brass disks) at  $(e, D_0, R, \nu) = (0.5, 3, 10, 10)$  in mm or St with the fitting lines in Fig. 3 (b), to clearly show the  $\Delta\rho$  dependence.

II (results of fitting are shown in the plot), although the range of regimes are limited (especially in Regime II).

### E. Self-similarity in the interface shape dynamics

In Fig. 4 (a1) to (a3), we show temporal changes of the interfacial shape after breakup for  $e = 0.5$  mm but with different  $\eta$ ,  $D_0$ , and  $R$ . As seen in Fig. 4 (b1) to (b3), interface shapes after rescaling both axes by  $h(z, t)R/z_m^2$  and  $(z - z_m)/z_m$  are clearly collapsed onto a master curve,

especially near the tip where  $(z - z_m)/z_m \lesssim 1$ . The collapse shown in (b) implies the following scaling form, which are universal even if  $\eta$ ,  $D_0$ , and  $R$  are changed in a limited range:

$$h(z, t) = \frac{z_m^2}{R} \Gamma \left( \frac{z - z_m}{z_m} \right) \quad (2)$$

As shown in Fig. 5 (a), the master curve near  $t = t_c$  is universal (and reproducible) beyond the linear region near the tip even if parameters  $D_0$ ,  $R$ , and  $\eta$  are changed in a limited range with  $e$  fixed to 0.5 mm. The univer-

sal master curve can be well described by the following expression

$$\Gamma(X) = aX + bX^2, \quad (3)$$

as demonstrated in Fig. 5 (b), where we obtain  $a = 1.26 \pm 0.03$  and  $b = 0.65 \pm 0.01$  by fitting the data at 60 ms in the range of  $X$  from 0 to 5.5. The linearity of the master curve near the tip is well confirmed in Fig. 5 (c). Note that the confirmation of the collapse by Eq. (2) becomes very difficult for the shape very close to  $t = t_c$ , such as those at  $t$  with  $t - t_c \lesssim 10$  ms, which is the order of the time resolution of our experiment limited by frames per second in capturing images. This is because  $z_m$  becomes very small and approaches the spacial resolution of our experiment, meaning that the error in estimating  $z_m$  becomes too large.

The collapse observed for the post-breakup dynamics ( $t > t_c$ ) in Fig. 4 is regarded as space-time dependent if we notice that, by the present rescaling  $h(z, t)R/z_m^2$  and  $(z - z_m)/z_m$ , shapes at times closer to  $t = t_c$  are more strongly magnified, since  $z_m$  becomes smaller as  $t \rightarrow t_c$ : (1) Near the tip ( $z = z_m$ ), the master curve is linear and the shape collapse to it persists for times rather away from the breakup ( $t = t_c$ ). (2) Away from the tip ( $z > z_m$ ), it is parabolic, but the collapse is limited only near the breakup time ( $t \simeq t_c$ ). The space-time dependence is summarized as

$$\Gamma(X) \simeq \begin{cases} X & (X \ll 1) \quad \text{for long time after } t = t_c \\ X^2 & (X \gg 1) \quad \text{only for short time after } t_c \end{cases} \quad (4)$$

The space-time dependent behavior of the master curve in Eq. (4) is preserved even if we change  $e$  and  $\Delta\rho$  in a certain range, as shown in Fig. 6 (a1) to (b2). However, the coefficients  $a$  and  $b$  in Eq. (3) depend on  $e$  and  $\Delta\rho$  as shown in Fig. 6 (a3), while they are universal for different  $D_0$ ,  $R$ , and  $\eta$  as shown in Fig. 5. In Fig. 6 (a3), the difference in the curve formed by the symbol  $\triangleleft$  and the solid curve demonstrates the  $\Delta\rho$  dependence, comparing the cases using brass and stainless disks with  $e$  fixed to 0.5 mm. In contrast, the difference in the curve shaped by the symbol  $\triangleright$  and the solid curve shows the  $e$  dependence, comparing the cases of  $e = 1.0$  and 0.5 mm with  $\Delta\rho$  fixed. We have also confirmed that the master curve at  $e = 0.75$  mm, for example, collapses onto neither the master curve at  $e = 0.5$  mm nor that at  $e = 1.0$  mm for a fixed  $\Delta\rho$ .

## II. DISCUSSION

### A. The incomplete university: partial persistence of memory

The independence of the master curve representing the self-similarity from the length scales  $D_0$  and  $R$  shown in

Fig. 5 (a) and dependence on  $e$  shown in Fig. 6 (a3) reveal a new category of the incomplete universality for the memory of singular dynamics discussed in Introduction. This is because these lengths are the scales that set the initial boundary conditions of the present problem. In the present case, the master curve loses the memory on the scales  $D_0$  and  $R$ , but retains the memory of the smallest scale  $e$ , which is quite natural from the viewpoint of scale separation, with remaining dependence on the material parameter on  $\Delta\rho$  (and independence from  $\eta$ ).

### B. The pre- and post-breakup dynamics

In the case of the viscous-capillary breakup of a bubble under no geometrical constraint, where the axisymmetric liquid-air interface is described by  $r = h(z, t)$  in the cylindrical coordinate  $(r, \theta, z)$ , the non-universal self-similar dynamics could directly continue from the pre- to post-breakup dynamics (see, e.g., Sec. 3.5.1 of [5]): the same self-similar structure is maintained, meaning that the factors for rescaling to achieve collapse onto the master curve are the same when expressed as a function of a dimensionless time  $|\tilde{t}'| \sim |t - t_c|$ . In other words, the pre- and post-breakup are both expressed as  $h(z, t) = |\tilde{t}'| \Gamma(z/|\tilde{t}'|^2)$ .

As for the confined and non-axisymmetric breakup of the present focus, the pre-breakup dynamics was studied in the previous studies [14, 15] and two distinct cases were reported. When  $D_0 > \kappa^{-1} = \sqrt{\gamma/\rho g} \simeq 1.8$  mm, as in the present case, the liquid-sheet is formed at the constriction point, which leads to the breakup. When  $D_0$  is smaller, the axisymmetric corn is formed which detaches from the disk without breakup. In both cases, the dynamics was found to be self-similar and the self-similar structure of the pre-breakup corresponding to the present case of  $D_0 > \kappa^{-1}$  was reported as  $h(z, t) = 2|\tilde{t}'| \Gamma(z/|\tilde{t}'|)$ , which is significantly different from Eq. (2), i.e.,  $h(z, t) \simeq |\tilde{t}'|^{2\Delta} \hat{\Gamma}(z/|\tilde{t}'|^\Delta)$ . This suggests the scenario for the continuation from the pre- to post-breakup could be quite different. In addition, for the pre-breakup, although the master curve for  $D_0 > \kappa^{-1}$  is shown to be independent of  $D$ ,  $R$ , and  $\eta$  in a certain range [14], the dependence on  $e$  has yet to be confirmed. The problem of the continuation and the dependence on  $e$  for the pre-breakup for  $D_0 > \kappa^{-1}$  will be discussed elsewhere in the near future.

### C. Physics at the level of dimensional analysis

We may regard the present problem as finding a solution for Navier-Stokes equation for a viscous liquid, neglecting the role of air. The boundary conditions may involve, in addition to  $R$ ,  $e$ , and  $D$ , the velocity of the tip at  $t = t_c$ , if we start to solve the post-breakup dynamics from  $t = t_c$ . The tip velocity is known to scale

with the falling velocity of the disk in the previous study on the pre-breakup dynamics [14]: The velocity is shown to scale as  $v_G \sim \Delta\rho g D^2/\eta$ , as a result of the balance of gravitational and viscous energy (per time) for the disk:  $\Delta\rho g R^2 D v_G \sim \eta(v_G/D)^2 R^2 D$  (for  $D \simeq D_0$ ). In addition, we see in Eq. (2) and (1) any dependence on  $\gamma$  but on  $\eta$ ,  $g$ , and  $\Delta\rho$ . Thus, we expect

$$h = f(t', z, \Delta\rho, \eta, g, R, e, D) \quad (5)$$

we have 9 dimensional variables, of which only 6 are independent, since the dimension of the unit of all variables can be derived from the three fundamental units, kg, m, and s.

From the Buckingham  $\pi$  theorem (see, e.g., Appendix C of [5]), we expect a relation  $\pi_0 = \Xi(\pi_1, \pi_2, \dots, \pi_5)$ , where  $\pi_i$ 's are 6 independent dimensional variables and  $\Xi$  is a dimensionless function. We select these dimensionless variables as follows. A natural characteristic scale in the  $z$  direction is  $z_m$ , from which we define  $\pi_1 = z/z_m - 1$ . A natural unit  $h^*$  (in the  $x$  direction) for  $h$  can be introduced through a curvature relation,  $1/R \sim h^*/z_m^2$ , from which we set  $\pi_0 = h/h^*$ . To select the remaining 4 independent variables, we focus on 4 length scales:  $l = \eta/(\Delta\rho g t')$ ,  $R$ ,  $e$ , and  $D$ , which are normalized by  $z_m$  to determine 4 dimensionless variables,  $\pi_2, \dots, \pi_5$ . In this way, to be consistent with our experiment, we may arrive at

$$h = \frac{z_m^2}{R} \Xi((z - z_m)/z_m, l/z_m, R/z_m, D/z_m, e/z_m) \quad (6)$$

Here, we may expect that near the breakup point where  $z_m \sim (t')^{\Delta'}$  with  $0 < \Delta' < 1$  is small so that the right-hand side of the equation becomes independent of the second to the fourth dimensionless variables (with  $l/z_m \rightarrow \infty$  and  $R/z_m, D/z_m \rightarrow 0$  but with a finite  $e/z_m$ ), by which Eq. (2) with remaining dependence on  $e$  is reproduced.

#### D. Importance of exploring symmetry

In critical phenomena, where universality plays a significant role as in the singular dynamics [16, 17] and *such universality emerges because the physics at large scales becomes so important*, a myriad of universality classes have been found by exploring symmetry and dimensionality, which has propelled the developments of modern physics in different sub-domains such as soft and hard condensed matter, non-equilibrium systems, and active matter [18–21]. Given this, the present study suggests a promising direction for the study on the singular dynamics widely observed in nature by exploring the symmetry in confined geometries and by drawing an analogy with critical phenomena. The present findings on the singular dynamics with broken axisymmetry have implications for understanding many natural phenomena and industrial processes involving confinement, encountered in a

various fields, from geology and petroleum industry to microfluidics with applications such as in medicine and biochemistry [22–25].

#### ACKNOWLEDGMENTS

This work was supported by JSPS KAKENHI Grant Number JP19H01859 and JP24K00596.

#### Appendix A: Experimental Details

The setup and experimental procedure is the same as those in the previous study [14] not on the post-breakup dynamics of the present focus but on the pre-breakup. We here summarize important points to realize high reproducibility. We need to achieve (1) the thickness  $e$  of the lubrication films on both surfaces of the disk to be equal, i.e.,  $e = (D - D_0)/2$ , as indicated in Fig. 1 (a), (2) the initial velocity of the metal disk to be zero at the entry, and (3) the contact angle of the surface of the disk to be zero. Accordingly, (1) we set a gate with the gap  $D_0$  at the top of cell by placing two small plates of thickness  $e$  on the inside surfaces of the cell, (2) we fall the disk so that the bottom of the disk is initially in contact with the air-liquid interface, and (3) we wipe the oil on the surface of the disk after dipping to coat the surface by a thin layer of the oil. To capture the dynamics, we analyzed the images with Image J and self-made Python codes, which were obtained with a high-speed camera (FASTCAM Mini UX 100, Photron) with a lens (Micro NIKKOR 60 mm f2.8G ED, Nikon) at 1000 to 2000 frames per second (fps).

#### Appendix B: Definitions of the shape function $h$ and setting of space-time coordinates

The inner edge by which we define the shape corresponds to the contact line on the front surface of the back cell wall, whose surface is totally wetting (thin layer of oil exists ahead of "the contact line"). The relation  $x = h(z, t)$  represents the shape outlined by the contact line on the back cell plate.

We here explain why the inner edge of the dark line corresponds to the contact line. In fact, the shape of the liquid-air interface is three dimensional: it should be a function of  $y$ :  $x = \tilde{h}(t, z; y)$  with  $h(z, t) = \tilde{h}(t, z; y = D)$ , where  $y = 0$  and  $y = D$  respectively correspond to the back surface of the front cell plate and the front surface of the back plate. This implies that the curvature  $\partial^2 \tilde{h}(t, x, z; y)/\partial y^2$  is negative (the surface of right branch is convex seen from the right liquid side), which goes to zero towards the tip: the outer edge corresponds  $x = \tilde{h}(t, z; D/2)$  where  $y = D/2$  corresponds to the middle plane between the inner surfaces of cell plates. This is because of continuity of surface, which is horizontal at

places far away from tip, where the surface should be concave seen from the upper air phase. In addition, the contact line at  $y = D$  is further away from the viewpoint compared with the line at  $y = 0$ , when seen from the front.

The critical time  $t_c$  used in the analysis was determined as follows. Towards breakup, the constriction region starts to form a thin thread (when seen from the front), which finally pinches off, by which moment, we define  $t = t_c$ . Precisely speaking, the pinch-off is judged not by the inner edge but the outer edge as indicated in Fig. 1 (b) left (the inner edge breaks up before the outer

edge), but the positions  $z_c$  and  $z_m$  are determined by the inner edge (In Fig.1 (b), these positions are actually slightly above the dashed horizontal lines by the amount of the thickness of the line representing the interface). In addition, we set the time label 0 ms as the snapshot just before the pinch off, using snapshots obtained at 1000 frames per second, which means there could be a difference at most 1 ms between our time label 0 ms and the actual critical time  $t = t_c$ . Because of this possible error in determining the origin of time, we avoid using snapshots too close to  $t = t_c$  and use only those at  $t \gtrsim 10$  ms.

---

[1] Matthew W Choptuik. Universality and scaling in gravitational collapse of a massless scalar field. *Physical Review Letters*, 70(1):9, 1993.

[2] XD Shi, M.P. Brenner, and S.R. Nagel. A cascade of structure in a drop falling from a faucet. *Science*, 265(5169):219, 1994.

[3] Tatsuhiko Koike, Takashi Hara, and Satoshi Adachi. Critical behavior in gravitational collapse of radiation fluid: A renormalization group (linear perturbation) analysis. *Physical Review Letters*, 74(26):5170, 1995.

[4] G. I. Barenblatt. *Scaling, self-similarity, and intermediate asymptotics*. Consultants Bureau, New York, 1979.

[5] Jens Eggers and Marco Antonio Fontelos. *Singularities: formation, structure, and propagation*, volume 53. Cambridge University Press, 2015.

[6] Benjamin W Zeff, Benjamin Kleber, Jay Fineberg, and Daniel P Lathrop. Singularity dynamics in curvature collapse and jet eruption on a fluid surface. *Nature*, 403(6768):401–404, 2000.

[7] Itai Cohen and Sidney R. Nagel. Scaling at the selective withdrawal transition through a tube suspended above the fluid surface. *Phys. Rev. Lett.*, 88(7):074501, Feb 2002.

[8] Maria Yokota and Ko Okumura. Dimensional crossover in the coalescence dynamics of viscous drops confined in between two plates. *Proc. Nat. Acad. Sci. (U.S.A.)*, 108:6395–6398; In this issue, PNAS, 108 (2011) 6337., 2011.

[9] JF Hernández-Sánchez, LA Lubbers, Antonin Eddi, and JH Snoeijer. Symmetric and asymmetric coalescence of drops on a substrate. *Physical Review Letters*, 109(18):184502, 2012.

[10] Paul R Kaneelil, Amir A Pahlavan, Nan Xue, and Howard A Stone. Three-dimensional self-similarity of coalescing viscous drops in the thin-film regime. *Physical Review Letters*, 129(14):144501, 2022.

[11] Jens Eggers. Universal pinching of 3d axisymmetric free-surface flow. *Phys. Rev. Lett.*, 71(21):3458, 1993.

[12] Pankaj Doshi, Itai Cohen, Wendy W. Zhang, Michael Siegel, Peter Howell, Osman A. Basaran, and Sidney R. Nagel. Persistence of memory in drop breakup: The breakdown of universality. *Science*, 302(5648):1185–1188, 2003.

[13] Amir A Pahlavan, Howard A Stone, Gareth H McKinley, and Ruben Juanes. Restoring universality to the pinch-off of a bubble. *Proceedings of the National Academy of Sciences*, page 201819744, 2019.

[14] Hana Nakazato, Yuki Yamagishi, and Ko Okumura. Self-similar dynamics of air film entrained by a solid disk in confined space: A simple prototype of topological transitions. *Physical Review Fluids*, 3(5):054004, 2018.

[15] Hana Nakazato and Ko Okumura. Air entrained into viscous liquid by a disk: Confinement induced suppression of breakup. *Physical Review Research*, 4(1):013150, 2022.

[16] J. Cardy. *Scaling and Renormalization in Statistical Physics*. Cambridge Univ. Press, Cambridge, 1996.

[17] N. Goldenfeld. *Lectures on Phase Transitions and the Renormalization Group*. Addison-Wesley Pub., Reading, 1992.

[18] Pierre-Gilles De Gennes and Pierre-Gilles Gennes. *Scaling concepts in polymer physics*. Cornell university press, 1979.

[19] Roberto Livi and Paolo Politi. *Nonequilibrium statistical physics: a modern perspective*. Cambridge University Press, 2017.

[20] Alexander Altland and Ben D Simons. *Condensed matter field theory*. Cambridge university press, 2023.

[21] Julien Tailleur, Gerhard Gompper, M Cristina Marchetti, Julia M Yeomans, and Christophe Salomon. *Active Matter and Nonequilibrium Statistical Physics: Lecture Notes of the Les Houches Summer School: Volume 112, September 2018*, volume 112. Oxford University Press, 2022.

[22] Andrea Parmigiani, Salah Faroughi, C Huber, Olivier Bachmann, and Y Su. Bubble accumulation and its role in the evolution of magma reservoirs in the upper crust. *Nature*, 532(7600):492–495, 2016.

[23] H.A. Stone, A.D. Stroock, and A. Ajdari. Engineering flows in small devices. *Annu. Rev. Fluid Mech.*, 36(1):381–411, January 2004.

[24] Saeed Shad, Majid Salarieh, Brij Maini, and Ian D Gates. The velocity and shape of convected elongated liquid drops in narrow gaps. *J. Petroleum Sci. Eng.*, 72(1):67–77, 2010.

[25] Shelley Lynn Anna. Droplets and bubbles in microfluidic devices. *Annual Review of Fluid Mechanics*, 48:285–309, 2016.